Numerical Modeling of Macrosegregation in Binary Alloys Solidifying in the Presence of Electromagnetic Stirring

GREGORY MICHAEL POOLE, MATTHEW HEYEN, LAURENTIU NASTAC, and NAGY EL-KADDAH

A model for predicting solidification and solute segregation of binary alloys undergoing electromagnetic stirring has been developed. A dual-zone formulation was employed to describe the velocity fields in the mushy region. The key feature of this model lies in its accounting for flow damping in the suspended particle region *via* turbulent interactions the crystallite surfaces. The damping force is given in terms of the turbulent kinetic energy, fraction solid, and the crystallite sphericity. The computed macrosegregation results for Al-4.5 pctCu alloy were validated against, and were found to agree with, experimental measurements. The effect of final grain size and frequency on segregation was also determined. This validated model represents a rigorous mathematical framework for describing the flow behavior and solute segregation in electromagnetically stirred melts.

I. INTRODUCTION

MAINTAINING a uniform distribution of alloying elements is extremely difficult in many casting processes due to solute redistribution during solidification (aka segregation). There are two principal forms of segregation, namely microsegregation and macrosegregation, which occur at different length scales. Microsegregation occurs at the crystallite interfaces due to differences in the solute solubility of the various phases, while macrosegregation results from convective transport of solute-enriched liquid. Each of these phenomena can lead to significant spatial solute variations and by corollary physical properties.

In recent years, macrosegregation control in electromagnetic (EM) stirring systems has garnered particular interest due to its widespread use in solidification processes to produce castings exhibiting fine-grained equiaxed structures.[1–5] Zhang *et al*.[6] found that EM stirring significantly reduced the degree of solute heterogeneity during continuous casting of Al alloy billets. Prescott and Incropera[7] found, both experimentally and numerically,[8] that intensifying EM stirring reduced overall macrosegregation *via* increased turbulent mixing. However, other studies, such as those of Budenkova *et al*.[9] and Griffiths and McCartney,[10] found that in certain cases EM stirring can also lead to the formation of regions with positive and negative segregation within the casting.

There have been substantial efforts to model segregation in EM solidification processes.[8,9,11–16] Doing so requires, above all, an accurate description of the turbulent velocity and EM field phenomena in the bulk liquid and two-phase "mushy" regions. Generally, modeling of the EM forces has been accomplished using approximate analytical solutions such as those found in References 17,18. Such solutions, however, can only be found if highly simplified geometries are assumed, and thus have minimal flexibility in their application.

The models for the flow in the mushy region may be divided into (i) single-zone[8,12,16,19] and (ii) dual-zone models.[9,15,20] Single-zone models treat the flow in the entire mushy region as that of a porous medium governed by Darcy's law. While such models accurately predict flow behavior for columnar solidification morphologies, they do not account for the presence of floating equiaxed crystallites commonly found in EM solidification systems.[21] Dual-zone models account for the floating crystallite phenomenon by relaxing the porous medium assumption at low fraction solid, treating the flow in this "suspended particle region" as that of a rheological slurry. There have been some efforts to incorporate turbulence into both the single-zone[8,12] and dual-zone model formulations.[9,15] However, none of these models have accounted for the crystallite interactions with the turbulent field, which are known to damp the flow.[22–24]

Recently, some of the authors[25,26] have proposed an improved dual-zone model formulation for turbulent EM stirred solidification systems. The model solves the EM field equations numerically in both the melt and adjacent conducting domains. Most importantly, however, the model also accounted for flow damping due to crystallite interactions with the turbulent eddies.

GREGORY MICHAEL POOLE, Graduate Student, and LAURENTIU NASTAC, Associate Professor, are with the Department of Metallurgical & Materials Engineering, The University of Alabama, P.O. Box 870202, NERC 3007, 251 7th Avenue, Tuscaloosa, AL 35487-0202. Contact e-mail: lnastac@eng.ua.edu MATTHEW HEYEN, Technology R&D Engineer-Automotive, is with the Novelis Inc. Global Research and Technology Center, 1950 Vaughn Road, Kennesaw, GA 30144. The late professor NAGY EL-KADDAH, formerly with the Department of Metallurgical & Materials Engineering, The University of Alabama, is deceased.
Manuscript submitted April 21, 2014.
Article published online May 21, 2014.

The objective of this work is to examine the applicability of this newly developed theoretical approach to measurements obtained from an experimental EM stirring system. A satisfactory interpretation of these measurements serves a twofold purpose. First, it represents a fundamental test of the model's capabilities; more importantly, however, it allows for an expanded application of the model to more sophisticated systems and operating conditions.

II. MODEL FORMULATION

The mathematical description for any EM stirred solidification system is given in terms of the momentum and continuity equations for fluid flow, the heat, and mass conservation equations for the temperature and solute fields, respectively, and the needed subsidiary relationships to calculate the Lorentz forces, Joule heating, and turbulence parameters. Since a substantial number of these equations have been given in previous publications,[25,26] the model formulation presented in this work will be that of a broad outline only.

A. *Electromagnetic Field*

In two dimensional systems, the mutual inductance method will be used due to its ability to easily solve for the EM field quantities in the molten metal domain and adjacent conducting media without the need to grid free space. In this method, the conducting region(s) with respective electrical conductivity, σ, are divided into elementary circuits of constant current density, $\mathbf{J}$. The current density in each circuit is given in terms of current densities of all of the other circuits by

$$\oint \mathbf{J}.d\mathbf{l}_i = -j\omega\sigma\left[\sum_{m=1}^{\text{metal}} M_{i,m}(\mathbf{J}\cdot\mathbf{S})_m + \sum_{c=1}^{\text{shields}} M_{i,c}(\mathbf{J}\cdot\mathbf{S})_c + \sum_{k=1}^{\text{coil}} M_{i,k}I_k\right], \quad [1]$$

where $\mathbf{S}$ and $\mathbf{l}$ are the respective lengths and surface areas of the elementary circuits, j is the square root of -1, ω is the angular frequency, and $M_{i,j}$ is the mutual inductance given by

$$M_{i,j} = \frac{\mu_0}{4\pi}\iint\frac{d\mathbf{l}_j \cdot d\mathbf{l}_i}{r'}. \quad [2]$$

From the current density, the magnetic flux density, $\mathbf{B}$, is given by

$$\mathbf{B} = -\frac{\nabla \times \mathbf{J}}{j\omega\sigma}. \quad [3]$$

B. *Fluid Flow*

For the three flow domains shown in Figure 1, the continuity momentum conservation equations are, respectively, given as

$$\nabla \cdot \mathbf{u} = 0, \quad [4]$$

$$\rho\frac{\partial\mathbf{u}}{\partial t} + \rho\mathbf{u}\cdot\nabla\mathbf{u} = -\nabla P + \mu\nabla^2\mathbf{u} + \lambda(\mathbf{J}\times\mathbf{B} + \mathbf{F}_{\mathrm{d}}) - \frac{\mu_{\mathrm{l}}}{K}(\mathbf{u} - \mathbf{u}_{\mathrm{s}}), \quad [5]$$

where

$$\mathbf{u} = f_s\mathbf{u}_s + (1 - f_s)\mathbf{u}_l \quad [6]$$

and ρ, $\mathbf{F}_{\mathrm{d}}$, and λ represent the density, turbulent damping force, and a switch parameter, respectively. The quantity $\mathbf{J} \times \mathbf{B}$ is the Lorentz force. In the bulk liquid and suspended particle regions, λ is equal to unity and is zero in the fixed particle region. Since it is assumed that the velocity of solid is equal to velocity of liquid in the bulk liquid and suspended particle region *via* the homogeneous flow model, the Darcy term is finite only in the fixed particle region. The flow permeability, K, was determined using the Carman–Kozeny equation, and the turbulent damping force is given by

$$\mathbf{F}_{\mathrm{d}} = \frac{2\left(1 - f_{\mathrm{L}}^2\right)\sqrt{c_{\mathrm{d}}}\rho k}{D_{\mathrm{g}}\left(1 - \left(\frac{6(1-f_{\mathrm{L}})}{\pi\beta}\right)^{1/3}\right)}\hat{\mathbf{e}}_{\mathrm{j}}, \quad [7]$$

where β is the sphericity of the crystallites. It should be noted that the coherency fraction solid, f_{c}, is equal to $6\pi/\beta$ for a simple cubic array of crystallites.

The turbulent characteristics of the flow were given by the low-Re k–ε model of Jones and Launder,[27] and the effective viscosity, μ, is given as the sum of the laminar and turbulent components, μ_{l} and μ_{t}, respectively. It is also assumed that turbulence is completely damped in the fixed particle region due to the interparticle spacing in this region being on the same order as the Kolmogorov turbulence length scale.[28] In the bulk liquid and fixed particle regions, the laminar viscosity component is equal to that of the molecular value, while in the suspended particle region the rheological effect on the laminar viscosity is represented using the correlation developed by Thomas.[29]

C. *Heat Transfer*

Assuming that the fraction solid, f_{s}, varies as a piecewise linear function of temperature, T, the differential energy balance equation with phase change is given by

$$\rho C^*\left(\frac{\partial T}{\partial t} + \mathbf{v}\cdot\nabla T\right) = \nabla\cdot(k^*\nabla T) + \frac{\|\mathbf{J}\|^2}{\sigma}, \quad [8]$$

where the last term accounts for electrical energy dissipation (aka Joule heating). The quantity C^* is the effective specific heat given in terms of the molecular specific heats of each phase, $c_{\mathrm{p,i}}$, the latent heat L, and the solidus and liquidus temperatures T_{S} and T_{L}, respectively, by
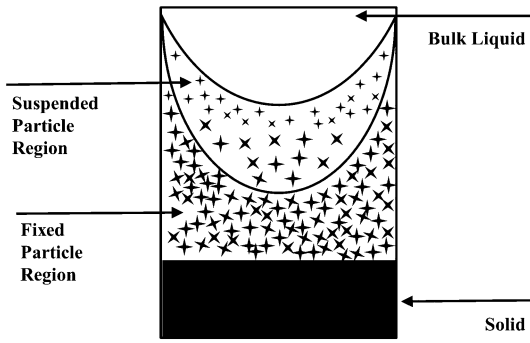
Fig. 1—Flow domains for the dual-zone solidification model.

$$C^* = \begin{cases} c_{p,l} & T \geq T_L \\ c_{p,s} + \frac{L}{T_i - T_j} & T_S < T < T_L \\ c_{p,s} & T \leq T_S \end{cases} \quad [9]$$

The quantities T_i and T_j represent the end point temperatures of a line segment of the piecewise linear curve. The effective thermal conductivity, k^*, is given by

$$k^* = \begin{cases} k_l + \frac{\mu_t c_{p,l}}{Pr} & T \geq T_L \\ (1 - f_S)k_l + f_S k_s & T_S \leq T < T_L \\ k_s & T \leq T_S \end{cases} \quad [10]$$

In the bulk liquid, the effective thermal conductivity is given by the sum of the turbulent and molecular contributions, where Pr is the turbulent Prandtl number.

D. Solute Segregation

For a binary alloy, the overall mass conservation equation for the solute species in a two-phase system is given by:

$$\frac{\partial}{\partial t}(\rho_s g_s C_s + \rho_l g_l C_l) + \nabla \cdot (\rho_s g_s \mathbf{v}_s C_s + \rho_l g_l \mathbf{v}_l C_l) \\ = \nabla \cdot (\rho_s g_s D_s \nabla C_s + \rho_l g_l D_l \nabla C_l). \quad [11]$$

The mass fraction solid, f_i, and the volume fraction solid, g_i, of a any particular phase are related by

$$f_i = \frac{\rho_i g_i}{\rho}. \quad [12]$$

Using Eq. [12], along with the assumptions made by Chang and Stefanescu,[30] Eq. [11] can be generally rewritten as

$$\rho f_L \frac{\partial C_L}{\partial t} + \rho f_L \mathbf{v}_L \cdot \nabla C_L = \nabla \cdot (\rho f_L D_L \nabla C_L) + \Omega, \quad [13]$$

where Ω is the solute rejection source term given by

$$\Omega = \begin{cases} \rho(1 - k_0)C_L\left(\frac{\partial f_s}{\partial t} + \mathbf{v}_s \cdot \nabla f_s\right) & 0 < f_s \leq f_c \\ \rho(1 - k_0)C_L \frac{\partial f_s}{\partial t} & f_c < f_s \leq 1 \end{cases}, \quad [14]$$

where k_0 is the equilibrium partition coefficient. Like the thermal conductivity, the mass diffusivity of the liquid is given as the sum of the molecular and laminar contributions:

$$D_L = D_m + \frac{\mu_t/\rho}{Sc} \quad [15]$$

where D_m is the molecular value of the liquid diffusivity, and Sc is the turbulent Schmidt number, generally taken to be approximately unity.[31]

III. RESULTS AND DISCUSSION

In this section, we will present the computed results for Al-4.5 pctCu alloy under unidirectional solidification in a bottom chill mold surrounded by an induction coil, along with a comparison with measured segregation profiles. The thermophysical properties used in the analysis are given in Table I. The calculations were performed on a 40 × 25 grid for the coil current and frequency used in a previous experiment,[32] with the dimensions of the system given in Figure 2. The calculations used a characteristic grain size of 200 μm and a coherency fraction solid of 0.2 ($\beta = 0.3821$), which is characteristic of highly aspherical crystallites.

A. Computed Results

Figure 3 shows the initial computed velocity field in the melt. As seen in this figure, the flow consists of one primary, counterclockwise recirculating loop, accompanied by a secondary, clockwise rotating flow loop near the free surface of the melt. It should be noted that this flow is similar to those found by the authors in Reference 25.

Figure 4 shows the computed initial turbulent field. Note that the turbulent field is presented in terms of the ratio between the turbulent and laminar viscosities ($\mu^* = \mu_t/\mu_l$). As expected, turbulence is strongest near the vortex center of the primary flow loop at approximately 190 times the molecular viscosity, where the shear strain rate is highest. This result suggests that

Table I. Thermophysical Properties for Al-4.5 pctCu

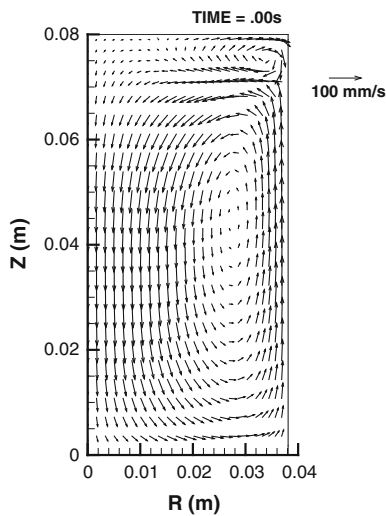|	
Solid density	2800 kg/m³
Liquid density	2300 kg/m³
Solid thermal conductivity	100 W/m °C
Liquid thermal conductivity	100 W/m °C
Solid heat capacity	1070 J/kg °C
Liquid heat capacity	1070 J/kg °C
Liquid mass diffusivity	3 × 10⁻⁹ m²/s
Electrical conductivity	1.28 × 10⁶ Mho/m
Liquidus temperature	921 K (648 °C)
Solidus temperature	837 K (564 °C)
Latent heat of fusion	389,000 J/kg
Molecular viscosity	1.5 × 10⁻³ Pa s
Initial temperature	675 °C
Heat transfer coefficient	250 W/m² °C
Grain geometry factor	0.3821
Characteristic grain size	200 μm
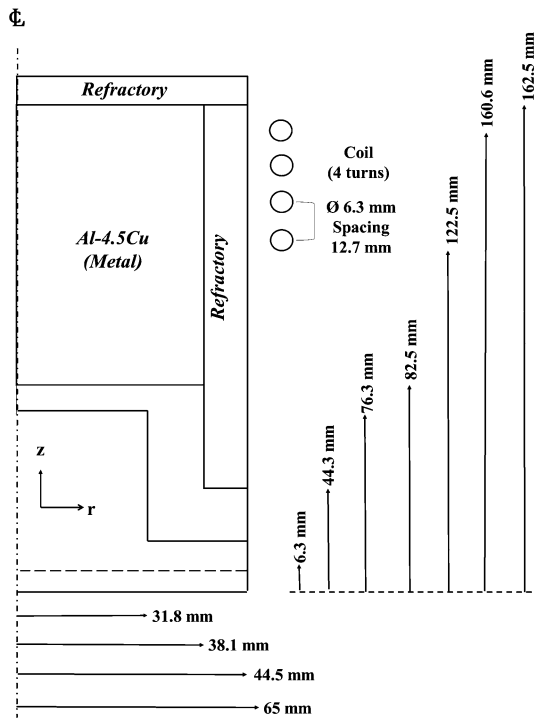
Fig. 2—Dimensions of the system used in this study.

Fig. 4—Initial turbulent field given in terms of turbulent to molecular viscosity.

Fig. 3—Initial computed velocity field; frequency 4900 Hz.

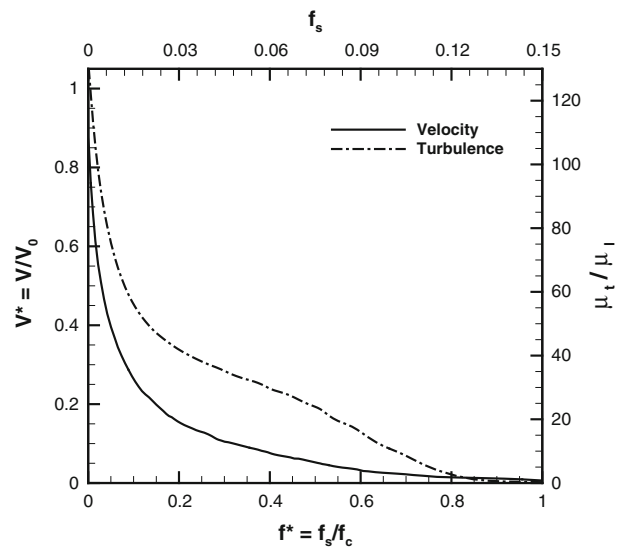

Fig. 5—Damping of the velocity and turbulent fields. Data taken at the centerline 20 mm from the chill.

there will be significant turbulent mixing in this region of the melt, leading to homogenization of both the temperature and solute fields during solidification.

As solidification progresses, there is significant damping of the flow in the mushy region due to the interaction of the turbulent eddies with the crystallites. This is clearly illustrated in Figure 5, which shows the variation of the velocity and turbulent fields with respect to fraction solid. The values presented for the velocity have been normalized with the value at zero fraction solid and the fraction solid is shown in terms of both normalized and actual values. The velocity decreases

rapidly in the initial stages of solidification ($f_s < 0.05$) due to the high values of turbulence; it then levels off at around 10 pct of its initial value near fraction solid of 0.03. The reason for this plateau is shown by the change in turbulent viscosity, where the decreased turbulent kinetic energy of the flow leads to smaller increases in the damping forces per unit of fraction solid.

Figures 6 and 7 show the liquid solute concentration profile at times of 360 and 550 seconds, respectively. After 360 seconds, Figure 6, the liquid concentration starts at ranges from 5.6 to 8.0 pct Cu and the solute concentration monotonically decreases with height at the outer radius. The solutal isolines tend to align themselves with the flow direction, due to the dominance of convective mass transport. It is also seen that the liquid composition in the interior of the ingot is more or
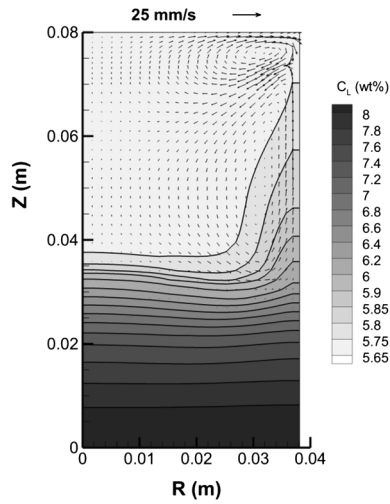
Fig. 6—Computed velocity and liquid solute profile after 360 s for frequency of 4900 Hz.
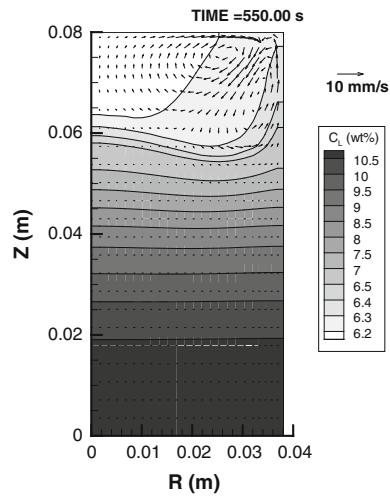

Fig. 7—Solute segregation profile after 550 s. Note the change of scale in the velocity.

less uniform in the suspended particle region due to the continued presence of turbulent mixing, similar to the computed results by Prescott and Incropera.[8] At 550 seconds, Figure 6, there are still two recirculating loops in the melt, but the secondary loop has shifted inward and has grown in size at the expense of the primary recirculating loop. Furthermore, damping of the flow has led to an increase in the solute gradient in the ingot interior. These results emphasize the importance of considering turbulent damping in the suspended particle region, as the resulting flow structures and intensities have a remarkable influence in solute field evolution.[25] This suggests that the final axial segregation profiles for any given radial value will be markedly different from one another.

The evolution of the computed axial concentration profiles, taken at the centerline for various times during solidification, is shown in Figure 8. It is clearly seen that the concentration starts at the initial value, C_0, of
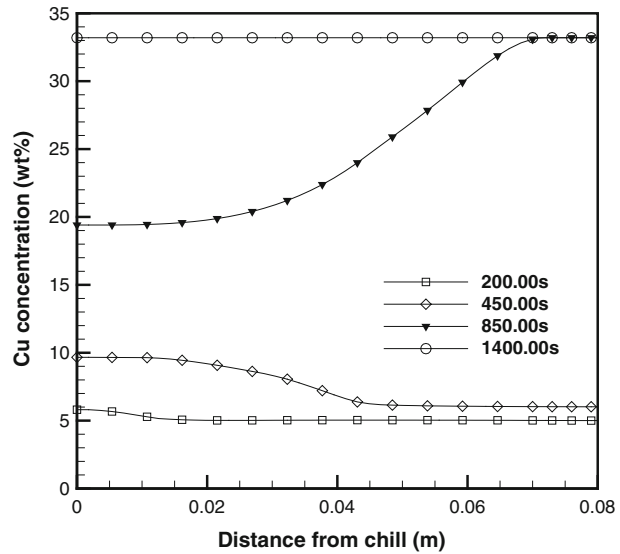

Fig. 8—Axial liquid concentration profiles, taken at the centerline for different stages of solidification.

4.5 pct Cu. As solidification progresses, the washing of solute due to intense convection in the suspended particle region, causing the curves to undergo an inflection near the middle of the axis height, as seen with the liquid composition curve for 850 seconds. This may be contrasted with the results of Chang and Stefanescu[30] on solidification of an Al-Cu alloy of similar composition, where the dominant shrinkage-driven flow caused significant inverse segregation. It should also be noted that those models which assume an complete solid diffusion[8,33,34] would only attain a maximum concentration of $C_0/k_0 = 26.16$ wt pct Cu, meaning that there should be no eutectic composition present at the conclusion of solidification. As shown in electron backscatter micrographs in Figure 9, this is clearly not the case, as there is a significant amount of eutectic outlining the dendrites.

The model was finally validated by comparing the final computed compositional profiles with measured data. As seen in Figure 10, there is good agreement between the predicted results and the measured stirred and unstirred solute profiles. It is also seen that stirring using a stationary magnetic field results in increased segregation along the ingot height. This result is again consistent with micrographs in Figure 9, where there is higher fraction of eutectic at 60 mm from the chill, Figure 9(b), compared to that at 20 mm, Figure 9(a). It is interesting to note that a similar result of monotonic segregation was found by Stelian et al.[35] for segregation of GaInSb alloy stirred using a stationary magnetic field. While not advantageous in ensuring homogeneous castings, these results suggest that stirring under these conditions may be useful in solidification processes where it is desirable to remove unwanted solute.

B. Influence of Fraction Solid Evolution

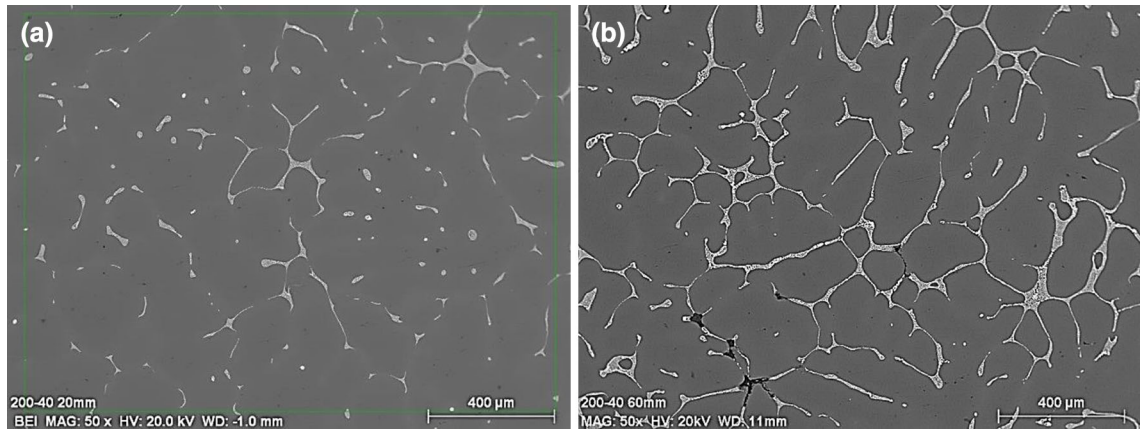It is also instructive to examine the influence of various model inputs on the final composition profile.

Fig. 9—Electron backscatter micrographs taken for EM stirred sample at (*a*) 20 mm and (*b*) 60 mm from chill block. Images taken at ingot centerline.
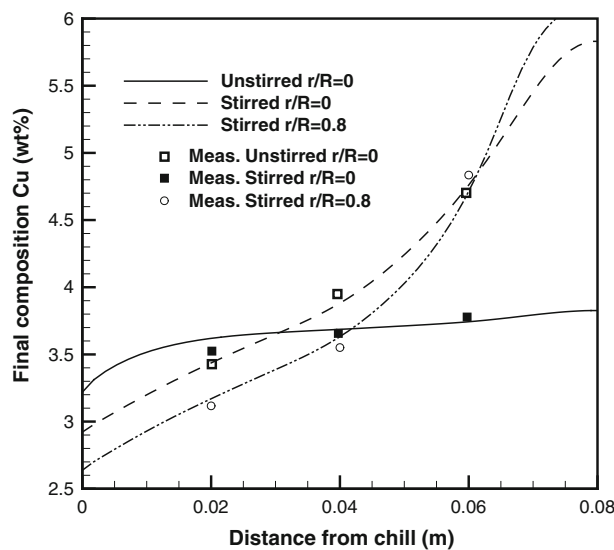

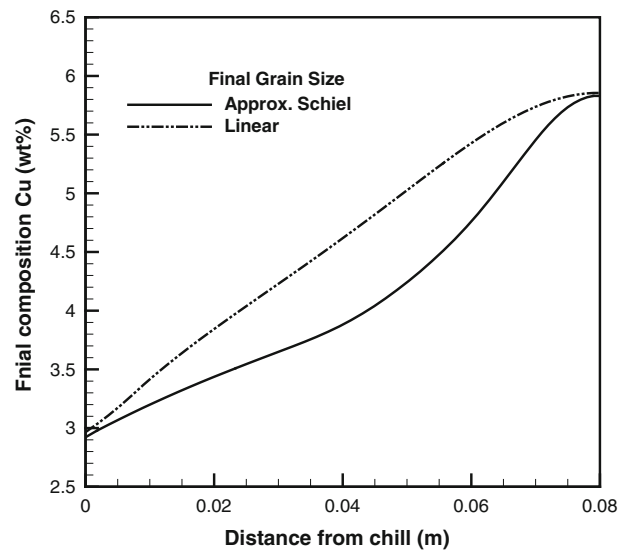Fig. 10—Final computed composition profiles at different radii compared with experimental measurements.

Fig. 11—Influence of assumed f_s *vs* T profile on the final solute composition at the centerline.

Figure 11 shows the final centerline composition curves for two different fraction solid *vs* temperature profiles. As seen in Figure 11, assuming a linear f_s *vs* T profile for heat transfer while using the Scheil assumptions for mass transfer, which has been done in other works,[30] leads to an overestimation of final composition compared to the piecewise Scheil curve due to the increased solute rejection from the solid into the liquid. This result shows the importance of using consistent assumptions in the solution of the temperature and solute conservation equations, as failure to do so will lead to spurious predictions.

Figure 12 shows the influence of final grain size on the final solute profile in the cast alloy. As seen in this figure, the amount of centerline segregation increases in the upper half of the casting for increasing grain size. As explained in the authors' previous work,[25] the increase in particle size reduces the specific surface area under which turbulent damping can occur, leading to increased

flow intensity and increases the washing of solute from other parts of the casting. The results shown here are also consistent with those in Figure 10, as the intensity of segregation decreases as the velocity of the flow tends to zero in the case of the unstirred melt, and is also consistent with previous experiments,[36,37] which showed decreased segregation in castings exhibiting highly refined grain structures.

The coil operating frequency had the most profound effect on solute segregation. As seen in Figure 13, segregation in the upper half of the ingot becomes more severe as the frequency decreases until 100 Hz, after which composition becomes more uniform. This is best explained by examining Figure 14, which shows the liquid composition profile after 360 seconds for a coil frequency of 500 Hz. As seen in this figure, decreasing the frequency by an order of magnitude causes an expansion of the upper recirculating loop in size such that it approximately covers the upper half of the ingot,
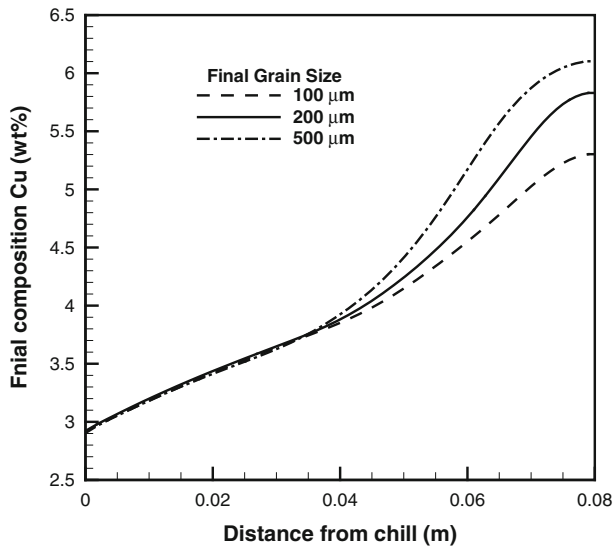
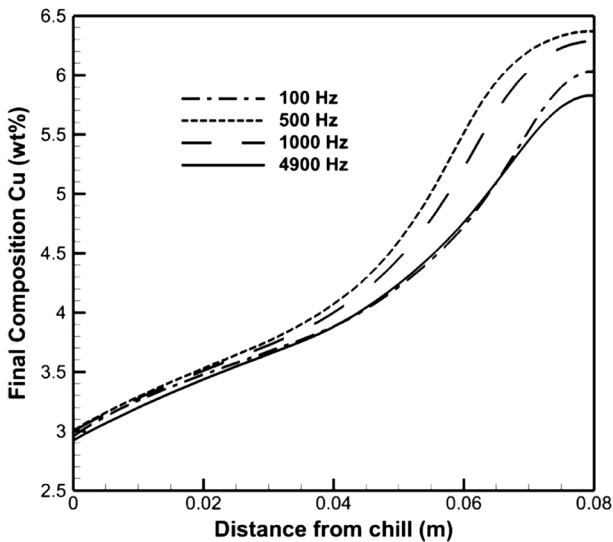Fig. 12—Influence of final grain size on the final centerline composition.

Fig. 13—Effect of frequency of centerline segregation.

while the flow in the lower recirculating loop has been damped significantly. Whereas the dominant, counter-clockwise flow recirculation at 4900 Hz caused rejected solute to be primarily taken up at the outer radius, Figure 6, the reversal of the flow direction in the upper loop, Figure 14, causes a solute buildup at the centerline for the upper half of the ingot, leading to greater incorporation of alloying elements into the solid phase. It should be noted, however, that decreasing the operating frequency causes a likewise decrease in the magnitude of the Lorentz forces in the melt. This counteracts the recirculation loop expansion effect and lessens segregation. Due to these opposing effects, these results suggest that it may be more suitable to use traveling magnetic fields when performing EM stirring at elevated frequencies to eliminate the upper recircu-
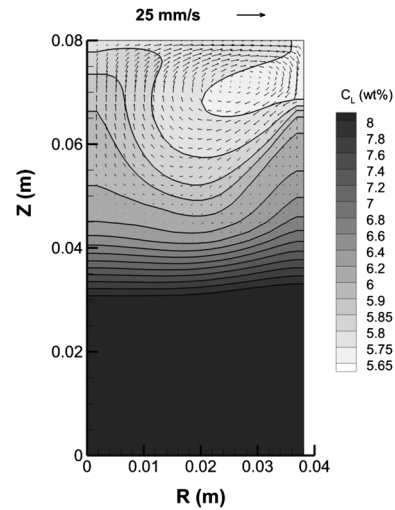

Fig. 14—Velocity and liquid solute concentration field after 360 s for frequency of 500 Hz.

lating loop or to use magnetic shields along with the stationary field to alter the flow structure.[38,39]

IV. CONCLUSIONS

A model for predicting solidification phenomena for binary alloys undergoing EM stirring has been presented. The EM field was solved using the mutual inductance technique, and a dual-zone formulation was employed to describe the velocity fields in the bulk liquid and mushy regions. The key feature of the model is that it accounts for the damping of the flow in the suspended particle region *via* the damping of turbulence at the crystallite surfaces, represented by a damping force given in terms of the turbulent kinetic energy and fraction of solid. The formulation for computing the solute field utilized a no solid diffusion assumption at the microscopic level. Computed results for the solidification of Al-4.5 pctCu alloy showed that segregation is strongest at the outer radius at the beginning of solidification, with washing of solute by the flow in the suspended particle region causing an inflection point to be reached as solidification progresses. The computed results were compared to, and were found to be in agreement with, experimental measurements. It was determined that the final grain size and coil operating frequency had the most profound effect on solute segregation. Therefore, it may be generally said that this model offers a rigorous mathematical framework for describing the flow behavior and solute segregation in electromagnetically stirred melts, and may be applied as a design tool to predict the behavior of other EM solidification processes.

REFERENCES

1. T. Campanella, C. Charbon, and M. Rappaz: *Scripta Mater.*, 2003, vol. 49, pp. 1029–34.
2. M. Paes, E.G. Santos, and E.J. Zoqui: *J. Achiev. Mater. Manuf. Eng.*, 2006, vol. 19, pp. 21–28.
3. A.N. Turchin, D.G. Eskin, and L. Katgerman: *Mater. Sci. Eng. A*, 2005, vols. 413–414, pp. 98–104.
4. N. Barman and P. Dutta: *Trans. Indian Inst. Met.*, 2012, vol. 65, pp. 683–87.
5. E. Jiang, E. Wang, G. Zhan, A. Deng, and J. He: in *Proceedings of 7th International Conference on Electromagnetic Processing of Materials*, Beijing, China, October 2012, pp. 313–316.
6. B. Zhang, J. Cui, and G. Lu: *Mater. Sci. Eng. A*, 2003, vol. 355, pp. 325–30.
7. P.J. Prescott, F.P. Incropera, and D.R. Gaskell: *Exp. Heat Transf. A*, 1996, vol. 9, pp. 105–31.
8. P.J. Prescott and F.P. Incropera: *J. Heat Transf.*, 1995, vol. 117, pp. 716–24.
9. O. Budenkova, F. Baltaretu, J. Kovács, A. Roósz, A. Rónaföldi, A.M. Bianchi, and Y. Fautrelle: *IOP Conf. Ser. Mater. Sci. Eng.*, 2012, vol. 33, p. 012046.
10. W. Griffiths and D. McCartney: *Mater. Sci. Eng. A*, 1996, vol. 216, pp. 47–60.
11. P.J. Prescott and F.P. Incropera: *J. Heat Transf.*, 1993, vol. 115, pp. 302–10.
12. W. Shyy, Y. Pang, G. Hunter, D.Y. Wei, and M.H. Chen: *Intl. J. Heat Mass Transf.*, 1992, vol. 35, pp. 1229–45.
13. J. Partinen, N. Saluja, J. Szekely, and J. Kirtley: *ISIJ Int.*, 1994, vol. 9, pp. 707–714.
14. R. Lantzsch: *J. Cryst. Growth*, 2007, vol. 305, pp. 249–56.
15. R. Pardeshi, A.K. Singh, and P. Dutta: *Numer. Heat Transf. A*, 2008, vol. 55, pp. 42–57.
16. S. Simlandi, N. Barman, and H. Chattopadhyay: *Trans. Indian Inst. Met.*, 2013, vol. 66, pp. 141–46.
17. K.H. Spitzer, M. Dubke, and K. Schwerdtfeger: *Metall. Trans. B*, 1986, vol. 17B, p. 119.
18. S. Milind and V. Ramanarayanan: *IEEE-IAS Conference*, 2004, pp. 188–94.
19. R. Mehrabian, M. Keane, and M.C. Flemings: *Metall. Trans.*, 1970, vol. 1, pp. 455–64.
20. C.M. Oldenburg and F.J. Spera: *Numer. Heat Transf. B*, 1992, vol. 21, pp. 217–29.
21. C.J. Parides, R.N. Smith, and M.E. Glicksman: *Metall. Mater. Trans. A*, 1997, vol. 28A, pp. 875–83.
22. Y. Yamagishi, H. Takeuchi, A.T. Pyatenko, and N. Kayukawa: *AIChE J.*, 1999, vol. 45, pp. 696–707.
23. J.L. Alvarado, C. Marsh, C. Sohn, G. Phetteplace, and T. Newell: *Intl. J. Heat Mass Transf.*, 2007, vol. 50, pp. 1938–52.
24. S. Wenji, X. Rui, H. Chong, H. Shihui, D. Kaijun, and F. Ziping: *Int. J. Refrig.*, 2009, vol. 32, pp. 1801–1807.
25. G.M. Poole and N. El-Kaddah: *Metall. Mater. Trans. B*, 2013, vol. 44B, pp. 1531–40.
26. G.M. Poole and N. El-Kaddah: *ISIJ Int.*, 2014, vol. 54, pp. 321–27.
27. W.P. Jones and B.E. Launder: *Intl. J. Heat Mass Transf.*, 1972, vol. 15, pp. 301–314.
28. H. Tennekes and J.L. Lumley: *A First Course in Turbulence*, MIT Press, Cambridge, 1972, pp. 19–20.
29. D.G. Thomas: *J. Colloid Sci.*, 1965, vol. 20, pp. 267–77.
30. S. Chang and D.M. Stefanescu: *Metall. Mater. Trans. A*, 1996, vol. 27A, pp. 2708–21.
31. J. Szekely and N. El-Kaddah: *Proceedings of International Seminar on Refining and Alloying of Liquid Aluminum and Ferro-alloys*, Trondheim, Norway, August 1985, pp. 249–66.
32. M.J. Heyen: MS Thesis, University of Alabama, Tuscaloosa, AL, pp. 21–40.
33. J. Chowdhury, S. Ganguly, and S. Chakraborty: *J. Phys. D*, 2005, vol. 38, pp. 2869–80.
34. K.C. Chiang and H.L. Tsai: *Int. J. Heat Mass Transf.*, 1992, vol. 35, pp. 1763–70.
35. C. Stelian, Y. Delannoy, Y. Fautrelle, and T. Duffar: *J. Cryst. Growth*, 2004, vol. 266, pp. 207–215.
36. G. Poole, N. Rimkus, A. Murphy, P. Boehmcke, and N. El-Kaddah: in *Proceedings of Magnesium Technology 2012*, Orlando, March 2012, pp. 161–64.
37. Y. He, A. Javaid, E. Essadiqi, and M. Shehata: *Can. Metall. Q.*, 2009, vol. 48, pp. 145–56.
38. J.L. Meyer, N. El-Kaddah, J. Szekely, C. Vives, and R. Ricou: *Metall. Trans. B*, 1987, vol. 18, pp. 529–38.
39. C. Vives and R. Ricou: *Metall. Trans. B*, 1985, vol. 16B, pp. 227–35.